UC San Diego
UC San Diego Previously Published Works

Title

Mechanical multi-level memory from multi-stable metamaterial

Permalink

https://escholarship.org/uc/item/4zq7r1x1

Journal

Applied Physics Letters, 122(21)

ISSN

0003-6951

Authors

Pechac, Jack E

Frazier, Michael J

Publication Date

2023-05-22

DOI

10.1063/5.0153438

Peer reviewed

Mechanical Multi-level Memory from Multi-stable Metamaterial on Elastic Foundation

Jack E. Pechac and Michael J. Frazier[a)]

Department of Mechanical and Aerospace Engineering, University of California, San Diego, California 92093, USA

(Dated: 9 February 2023)

In this letter, we couple a multi-stable metamaterial to an elastic foundation to realize a mechanical system within which the position of a transition wavefront can be precisely controlled and remotely determined. This ability is enabled, in part, by a (strain-)tunable potential energy landscape which conveys the wavefront from one stabilizing defect site to another. In separating two, acoustically distinct domains, the wavefront reflects small-amplitude waves of appropriate frequency back toward the source whereupon the time interval between excitation and echo reveals the position of the front. In a combined theoretical and numerical study, we exploit these mechanisms for mechanical multi-level memory which may find application, e.g., in soft robots as a flexible alternative to current rigid memory technologies. In general, we anticipate that the concepts presented here for a command of the transition wave position will further the development and applicability of multi-stable metamaterials.

(Multi-)ferroics[1] are crystalline materials whose unit cells notably exhibit multiple, energetically-equivalent stable configurations (i.e., phases, states) distinguished by one or more order parameters and, possibly, by unique physical properties. Within a given sample, each stable configuration may appear simultaneously, organized into regions of uniform phase (i.e., domains) separated by an interface (i.e., domain wall). Under the influence of a conjugate field[2], the domain wall may become mobile, transforming the local configuration in its path; thus, constituting a transition wave. These attributes hold considerable promise for nano-electronics applications[3], including, e.g., high-density memory[4] and re-configurable circuits[5,6]. The former interprets two given configurations as bits "0" and "1" while the latter leverages the enhanced conductivity of the domain wall (i.e., transition wavefront) and its ability to be re-positioned. Apparently, the manipulation of domains and domain walls in (multi-)ferroics is critical to developing their functionality and, therefore, remains an active area of research in condensed matter physics. A persistent challenge, however, lies in accessing the relevant length/time scales for precision control.

Recently, similar physics has been elicited at the structural level from mechanical metamaterials whose 3D-printable unit cells realize a non-convex potential function in a strain/displacement order parameter[7]. Numerous studies have been devoted to characterizing the motion of domain walls under various conditions[8–13]. In particular, Hwang and Arrieta[10] show monotonically decreasing elastic potentials to support uni-directional, multi-mode propagation which enables phase reversals. Jin *et al.*[14] demonstrate the utility of "hard" point defects (i.e., unit cells storing no deformation energy) in controlling the speed/direction and contour of a transition wavefront in a 2D environment. Together with an understanding of the physics of transition waves, the enhanced accessibility of the metamaterial internal architecture permits a tailorable response that has, so far, inspired proposals for, e.g., locomotion[15–17], signal transmission[9,18], tunable acoustic filtering[19], and mechanical logic operations[20] which promise flexible, mechanical alternatives to rigid electronics in otherwise soft robots and smart structures.

Inspired by these earlier works, in this letter, we propose a structural design leveraging a multi-stable metamaterial for mechanical multi-level (i.e., high-density) memory functionality. The concept may find utility in soft robotics, especially, the emerging paradigm of physical reservoir computing[21]. The basic operation of the proposed memory element – supported by theoretical and numerical analysis – relies on both large- and small-amplitude dynamics of the metamaterial: the former (transition waves) for the write operation and memory stability; the later (harmonic waves) for the read operation. The proposed design, method, and results are distinct from similar implementations of multi-stable architectures for mechanical (i.e., low-density) memory that, conversely, do not support transition waves and store only one bit per cell[22,23].

Figures 1a,b display schematics of the proposed mechanical multi-level memory element, comprising two discrete, one-dimensional chains, i.e., the *substrate* (SS) and the *metamaterial* (MM), with periodic and uniform inter-site coupling, $s_{j+1/2}$ and k_r, respectively. The two chains are connected locally through a non-linear spring (henceforth, associated with the metamaterial) adhering to the non-convex potential, $\psi(\Delta_j)$, $\Delta_j = v_j - V_j$, providing for the formation of transition waves. The system is an adaptation of the LOC arrangement utilized by Ramakrishnan and Frazier[19] for spontaneous alterations to the effective stiffness distribution in metamaterials. The corresponding non-dimensional

[a)]Corresponding author email: mjfrazier@ucsd.edu

Lagrangian is given by [SI]

$$\mathcal{L} = \sum_{j=1}^{N} \left[\frac{1}{2}(\dot{v}_j^2 + \dot{V}_j^2) - \alpha_j \psi(\Delta_j) \right] - \cdots$$

$$\frac{1}{2}\sum_{j=1}^{N-1} \left[(v_j - v_{j+1})^2 + s_{j+1/2}(V_j - V_{j+1})^2 \right],$$

from which the governing equations (with on-site viscous damping, η) of an arbitrary site j are derived as

$$\ddot{v}_j + \eta\dot{v}_j + (2v_j - v_{j+1} - v_{j-1}) + \alpha_j \frac{\partial\psi(\Delta_j)}{\partial v_j} = 0, \quad (1a)$$

$$\ddot{V}_j + \eta\dot{V}_j + s_{j+1/2}(V_j - V_{j+1}) + \cdots$$
$$s_{j-1/2}(V_j - V_{j-1}) + \alpha_j \frac{\partial\psi(\Delta_j)}{\partial V_j} = 0, \quad (1b)$$

where $\alpha_j = (1 + \gamma j)[1 + \beta\delta_{ij}]$ is a positive scalar responsible for effecting (i) the element-wide amplification/attenuation of the on-site potential as prescribed by the parameter, $\gamma = (-\infty, \infty)$, and (ii) the nature and distribution of "soft" point defects (i.e., unit cells storing anomalous deformation energy) as controlled by the parameter, $\beta \in (-1, \infty)$, and the Kronecker delta, $\delta_{Ij}, I = \{j|(j/J) \in \mathbb{N}\}$ with period $J \in \mathbb{N}$.

In order to elicit the desired functionality, the system adheres to certain design requirements. For one, $\psi(\Delta_j)$ possesses $n \geq 2$ degenerate ground states, $\Delta_j = \{\Delta_{s1}, \Delta_{s2}, \ldots, \Delta_{sn}\}$, supporting the formation of a (anti-)kink wave profile, yet, is asymmetric such that the linear on-site stiffness about each ground state, $k_{si} = \psi''(\Delta_{si})$, is unique (Fig. 1c.i). For another, the α_j vary monotonically (here, linearly) across the element except at p periodically-distributed defect sites, I, where, for $\beta < 0$ ($\beta > 0$), α_j is less (greater) than the neighboring $\alpha_{j\pm1}$ in order to create a locally attractive (repulsive) potential suitable for immobilizing transition waves. The monotonic variation otherwise supports the uni-directional propagation of both kink and anti-kink modes[10], permitting the present state, acquired by the passage of one transition wave, to be reversed by the passage of another of the opposite topological charge. The soft defects divide the system into p levels of J unit cells, each of which may be assigned an m-bit binary value where $m = \lfloor \log_2(p) \rfloor$ (Fig. 1a). Finally, although the substrate is pliable, proper function requires $s_{j+1/2}$ to be, effectively, rigid in comparison to $k_r (\equiv 1$ when non-dimensionalized) and k_{si}, i.e., $\min(s_{j+1/2}) \gg \max(k_r, k_{si})$. This relative rigidity ensures that the inhomogeneous strain that arises in the substrate upon the application of a prescribed boundary displacement is, effectively, reproduced in the metamaterial. Moreover, the stark difference in compliance allows for the dynamics of the metamaterial subsystem to treated in isolation at low frequencies, i.e., described by Eq. (1a) with a foundation of fixed V_j. Of the myriad possible periodic functions, the substrate
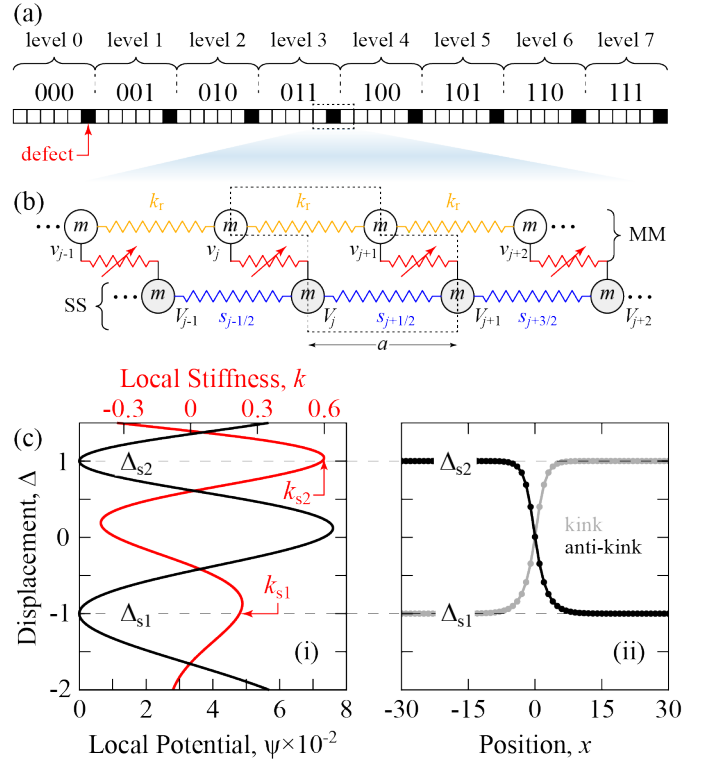

FIG. 1. Mechanical multi-level Memory. (a) Schematic of the mechanical (8-bit) memory element comprising p levels of J unit cells, including a defect cell. Each level is assigned a binary-encoded value for 0 to $p - 1$. (b) Detail of three unit cells (lattice constant a) of the substrate and metamaterial (MM) mass-spring chains comprising the element and locally coupled via non-linear springs generating a non-convex potential. (c) (i) The non-convex on-site potential (black) and corresponding local stiffness (red) supporting the formation of (ii) transition wavefronts separating domains of opposing ground state configurations, Δ_{si}, with characteristic on-site stiffness, k_{si}.

stiffness is modulated by a triangle wave

$$s_{j+1/2} = \frac{2(s_{\max} - s_{\min})}{J_s} \cdots$$
$$\times \left| \left(j - j_0 - \frac{J_s}{2} \right) \mod(J_s) - \frac{J_s}{2} \right| + s_{\min} \quad (2)$$

with period, J_s, offset, j_0, and minimum (maximum) value set by $s_{\min}$ ($s_{\max}$).

Consider, for example, the case in which $\gamma, \beta < 0$ such that α_j progressively reduces the on-site potential and establishes an energy well at the defect sites. A transition wave initialized at the left boundary will propagate to the right with constant speed[10,12] until entering and, with the aid of dissipative effects, becoming pinned (i.e., immobilized) within the potential well established by a soft defect. However, as discussed below, deforming the substrate modifies the energy landscape governing the transition wave motion, providing a mechanism for de-pinning and mobilizing the wave, even if only to

TABLE I. Parameters

	metamaterial			substrate		ψ			
	γ	β	J	J_{s}	j_0	a	b	c	d
Case I	-2.5×10^{-4}	$-1/5$	100	200	81	0.2582	0.0172	7.4489	0.0061
Case II	$-1.\bar{3}\times10^{-4}$	$-1/20$	25	50	17	0.2582	0.0172	7.4489	0.0380

become pinned again at the next defect site. The pinned position of the wavefront may be determined from the time of flight of a small-amplitude harmonic signal initiated at either boundary and reflected off the front due to the incompatible dynamics of the domains (i.e., regions of homogeneous Δ_{si} and k_{si}) that it separates. Thus determined, the current memory state is revealed as the number of consecutive levels in the configuration arbitrarily designated as, e.g., the "active", "ON", or "1" phase (here, Δ_{s2} is active); the opposing configuration fittingly labeled the "inactive", "OFF", or "0" phase. The element is the mechanical analogue of an electron CTF memory cell, where the two mechanical phases are likened to two charge states; J cells and defect sites are, respectively, likened to floating gates and isolators; mechanical load likened to voltage. Altogether, controlling and reading the defect-stabilized position of the domain wall enables a multi-level memory functionality.

In this letter, we define $\psi(\Delta_j) = d\{1 - \cos[a(\Delta_j + c) + b(\Delta_j + c)^3]\}$, where a, b, c, and d are tuning parameters that maintain an asymmetric potential with degenerate ground states distinct in k_{si}. In practice, these qualities may be realized, e.g., through the proper arrangement and orientation of magnetic di-poles[19].

The non-linearity of the metamaterial admits tailoring its dynamic response by straining the memory element, which alters the characteristic energy landscape dictating transition wave motion[24]. To illustrate this effect, we calculate the total potential energy, $\mathcal{U}(X_j)$, of the metamaterial in a finite system under various levels of prescribed strain as a function of the instantaneous position, $X_j = j$, of a (anti-)kink wavefront. In particular, we consider a system of $N = 200$ unit cells constructed following the set of parameters given in Case I of Table I. For analytical convenience, $|\gamma|$ is chosen sufficiently small to ensure that the supported (anti-)kink exhibits a (effectively) permanent profile while traveling the length of the system and that the k_{si} are (effectively) independent of position. For this and the following studies, the extrema of the substrate stiffness variation adhere to $s_{\max} : s_{\min} = 3 : 1$.

Following a prescribed boundary displacement, the interiors of the metamaterial and substrate each acquire new equilibrium configurations, v_j^0 and V_j^0. While $\mathcal{U}(X_j)$ may be computed via simulation, this approach yields an incomplete picture when the simulated transition wave becomes pinned, preventing the energy from being evaluated beyond X_j. It is more effective to utilize an analytical model with prescribed X and the continuum form of the total potential energy [SI]

$$\mathcal{U}(X) = \int_0^\ell \left[\alpha(x)\psi(v) + \frac{1}{2}\left(\frac{\partial v}{\partial x} + \frac{\partial v_0}{\partial x}\right)^2 \right] \mathrm{d}x, \quad (3)$$

where $\ell = Na$, and $v_0(x)$ and $V_0(x)$, respectively, model the initial strain-induced equilibrium displacements of the metamaterial and substrate. In general, exact analytical expressions for $v(x; X)$, $v_0(x)$, and $V_0(x)$ are difficult to obtain from the corresponding continuum governing equations; therefore, they are approximated by fitting ansatzes to the discrete results from simulation of Eq. (1). As the wave profile is assumed constant across the memory element, we fit $v(x; X) = A \arctan\left[B_1 e^{C_1(x-X)} + B_2 e^{C_2(x-X)}\right]$ to the simulated (anti-)kink at rest in an unstrained, uniform system [i.e., $(\gamma, \beta) = (0, 0)$] [SI]. For the initial equilibrium displacements, the fitting function combines a linear function and a qth-order Fourier expansion:

$$v_0(x) = a_0 + c_0 x + \sum_{n=1}^q a_n \cos(nx) + \sum_{n=1}^q b_n \sin(nx),$$

where the fitting function for $V_0(x)$ has the same form. For all studies, we find good agreement between fitted curves and simulation results, limiting the root-mean-square error to $e_{\mathrm{rms}} < 1.35 \times 10^{-4}$.

Figure 2a plots $\mathcal{U}(X)$ for various levels of initial substrate strain, $\varepsilon = \Delta\ell/\ell$, which may be physically achieved via, e.g., pneumatic actuation with flexible plumbing, electric actuation with an electro-active polymer composing the substrate, or direct mechanical loading. Here, we simply prescribe $V_1 = 0$ and $V_N \neq 0$. For $\varepsilon = 0$, there is a pronounced decrease in the potential energy centered at the location of the soft defect ($x = 0$) as α locally lowers the energy expenditure for switching between stable states, representing a local attractor which, aided by dissipative effects, may pin an incoming transition wave. As $|\varepsilon|$ increases, the defect energy well shallows; consequently, the attractor is less able to pin incoming waves and already pinned waves are more susceptible to mobilization by external perturbation. In addition, $\mathcal{U}$ develops strain-dependent local extrema associated with locations where the gradient of the substrate stiffness modulation changes sign (e.g., the peak or trough of a triangle modulation) which, appropriately, either attract or repel the transition wave and, in doing so, alter the speed/direction of its
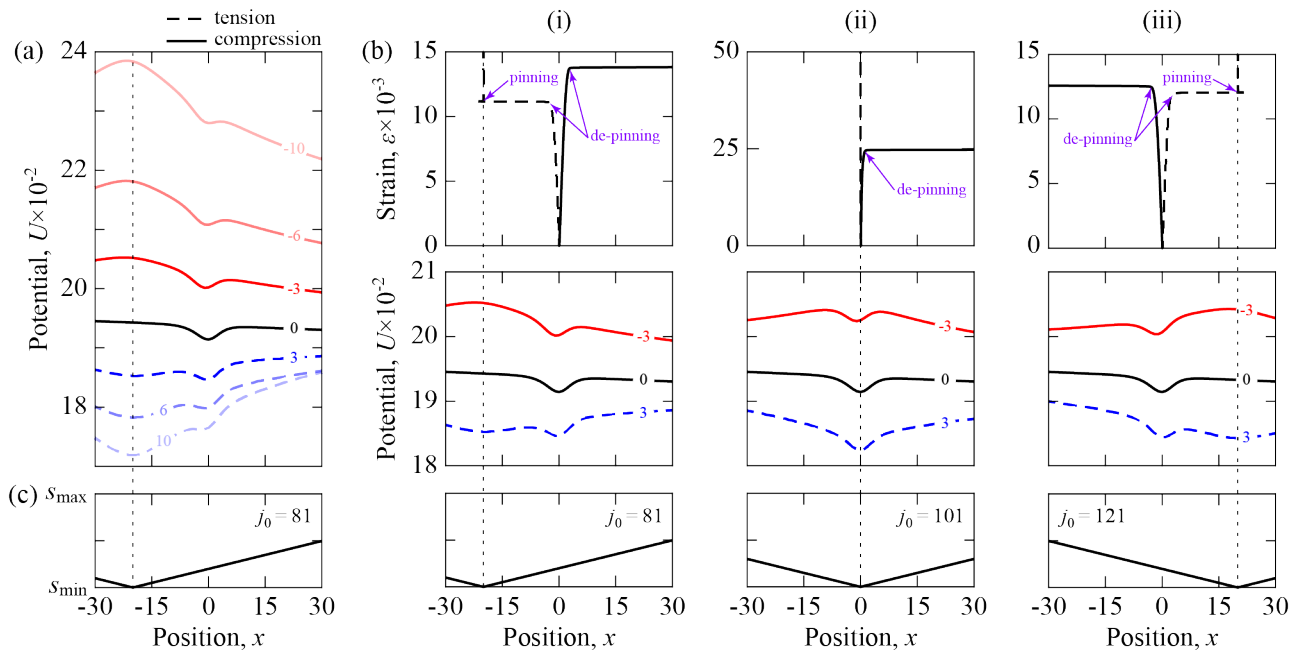
FIG. 2. Strain-tunable Energy Landscape. (a) The energy landscape, $\mathcal{U}(X)$, encountered by a transition wave in the proposed system under compressive and tensile pre-deformation. Under deformation, local energy extrema develop, reducing the pinning ability of the soft defect energy well which, ultimately, promotes de-pinning. Embedded curve labels indicate the strain, $\varepsilon \times 10^{-3}$. (b) The simulated position of an initially-pinned anti-kink as the applied strain increases quasi-statically, revealing instances of de-pinning and re-pinning in accordance to the changing profile of $\mathcal{U}(X)$ for $s_{\min}$ located (i) before, (ii) at, and (iii) after the soft defect. (c) Profile of the substrate stiffness.

propagation. For the current system, under compression (tension) a local maximum (minimum) develops in the vicinity of $s_{\min}$; the opposite effect (not shown) manifests in the vicinity of $s_{\max}$. The observed distortion in $\mathcal{U}$ reflects the work done by the non-uniform load applied to the metamaterial by the deformed substrate, revealing pre-strain as a mechanism for spontaneously altering the dynamics of transition waves in a host medium, post-fabrication. For the (anti-)kink initially pinned at $x = 0$, sufficient strain will effectuate de-pinning and mobilization; although, due to the asymmetries inherent to $\alpha(x)$, as well as the phase difference between δ_{Ij} and the substrate stiffness modulation, the critical strain at which this occurs and the direction of propagation depends on the deformation mode. These effects are illustrated in Fig. 2b. The first row of Fig. 2b tracks the simulated position the anti-kink wavefront initially pinned at $x = 0$ as $|\varepsilon|$ quasi-statically increases. For a sufficient strain, energy extrema *not* aligned with the defect location, ultimately, induce de-pinning and compel the newly-liberated wavefront to seek an another potential minima, which is achieved by propagating to either the system boundaries or a strain-induced minima whereupon it is pinned again (Fig. 2b.i,iii). For a sufficient strain, de-pinning and propagation may still occur when the maxima is aligned with defect location – though, under a significantly higher magnitude of strain – due to the asymmetry established by $\alpha(x)$ (Fig. 2b.ii).

Altogether, these results demonstrate the utility of soft defects and prescribed strain in modifying the energy landscape to effect the pinning, de-pinning, and propagation speed/direction control of transition waves which we exploit for mechanical multi-level memory.

Turning our attention to the propagation of small-amplitude harmonic signals, for the hypothetical scenario of an infinite, undeformed system of homogeneous ground state configuration, the application of Bloch's theorem to the linearized and lossless form of Eq. (1a) yields the characteristic dispersion relations for small-amplitude waves confined to the metamaterial [SI]:

$$2 + k_{\text{s}i} - \frac{1}{\vartheta} - \vartheta = \omega^2, \tag{4}$$

where ω is the dimensionless temporal frequency and $\vartheta = \mathrm{e}^{\mathrm{i}\kappa a}$ is the propagation constant with dimensionless complex wavenumber, κa. In formulating Eq. (4), we have assumed $(\gamma, \beta) = (0, 0)$, which is reasonable in the scenario where (as is the case here), in constructing the (finite) mechanical memory element, both γ and β are kept small as are the number and density of pinning sites, and the size of the system does not result in a large discrepancy between corresponding $k_{\text{s}i}$ at each boundary. In solving Eq. (4) for $\vartheta(\omega)$, propagating and attenuating wave modes are extracted, respectively, as $\kappa_{\text{R}} a = |\mathrm{Re}(\mathrm{i}\ln\vartheta)|$ and $\kappa_{\text{I}} a = |\mathrm{Im}(\mathrm{i}\ln\vartheta)|$. Figure 3a displays the dispersion curves for a system consistent
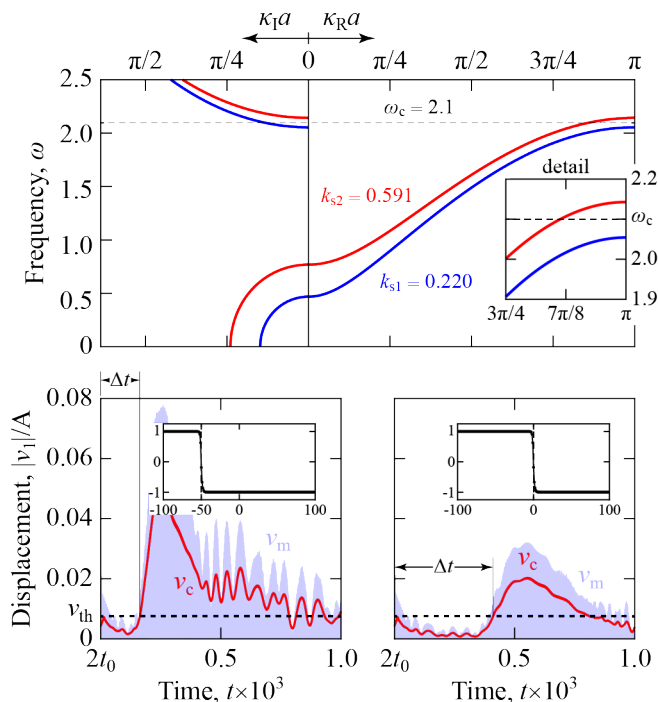
FIG. 3. Dynamics of Small-Amplitude Waves. (a) The propagating and attenuating frequency bands of the metamaterial homogeneous in state Δ_{s1} (red) and state Δ_{s2} (blue). (b) History of a harmonic pulse (according to v_1) injected into the metamaterial with transition wave (insets) pinned at different locations: (i) $j = 51$ and (ii) $j = 101$. The elapsed time, Δt, between signal injection and echo (threshold, $v_{th} = 7.5 \times 10^{-3}$) correlates to the distance between the injection site ($j = 1$) and the transition wavefront. (a) Infinite and (b) finite models consistent with Case II, Table I.

with Case II of Table I, revealing the non-overlapping frequency ranges of the respective propagating modes.

For the finite system supporting a pinned transition wave which separates domains with unique k_{si}, the results in Fig. 3a suggests that a propagating signal stimulated in one domain cannot enter the second domain if the Fourier components are not supported there. Instead, at the domain wall, the wave energy is reflected back toward the source as an echo. To demonstrate this, we simulate the response of a finite system ($N = 200$) to a Gaussian-modulated harmonic pulse stimulated within the metamaterial where a pinned anti-kink separates opposing regions of k_{s2} (left) and k_{s1} (right). For an excitation at the left end, the displacement prescription has the form:

$$v_1(t) = \begin{cases} v_{s2} + A\exp\left[-\frac{1}{2}\left(\frac{t-t_0}{\sigma}\right)^2\right]\sin(\omega_c t), & t \leq 2t_0 \\ \\ \text{not prescribed}, & t > 2t_0 \end{cases}$$

where ω_c and σ are, respectively, the carrier frequency

and the standard deviation. The corresponding velocity at the left boundary, $\dot{v}_1(t)$, is also enforced. In particular, the carrier frequency is restricted to lie within the propagating band associated with the designated active configuration. Here, we select $\omega_c = 2.4$. For the Gaussian envelope, $\sigma = 8$ and $t_0 = 6\sigma$. As only the small-amplitude response is of interest, we limit the excitation amplitude to $A = 0.01$. For the numerical analyses, we apply the Noh-Bathe integration scheme[25] to Eqs. (1) with $\eta = 1/250$. Figure 3b plots both the resulting displacement magnitude, $v_m(t) = |v_1(t)|$, and its smoothened, time-averaged counterpart defined by the convolution, $v_c(t) = [v_m \cdot h](t)$, where $h(t)$ is a rectangular window function of width, $T = 16\pi/\omega_c$, centered at t. Naturally, the elapsed time, Δt, between signal generation and the returned echo [identified by $v_c(t) > v_{th}$ for $t > 2t_0$, v_{th} a threshold value] changes with distance between the boundary excitation (i.e., the source) and the domain wall. This correlation is exploited in the mechanical multi-level memory element to infer the location of the pinned domain wall and, thus, identify the current memory state.

We bring together the physics of small- and large-amplitude waves, of soft defects, as well as the ability to tune the energy landscape in order to assemble a mechanical system with multi-level memory functionality, which we demonstrate numerically. Specifically, we simulate the response of an anti-kink within a metamaterial-substrate system ($N = 225$) under deformation due to a prescribed, quasi-static boundary displacement. The relevant parameters are listed in Case II of Table I, imbuing the metamaterial sub-system with eight pinning sites sufficient for 3-bit memory storage.

Figure 4a.i, an xt-contour diagram of the configuration, Δ_j, depicts the controlled advancement of a transition wave across the memory element as the system undergoes cycles of prescribed compressive, tensile, and zero strain (Figure 4a.ii). The transition wave is initially pinned at $x = -75$, representing level 0 with binary code 000. In practice, a (anti-)kink or harmonic pulse may be injected from the boundary with the aid of a solenoid actuator coupled to the boundary site. Under a non-zero strain, a change in the energy landscape releases and repels the domain wall from its current pinned position and toward another pinning site. Upon recovery of the zero strain condition, the transition wave becomes pinned at a soft defect site different from the one from which it originated (presently, the subsequent pinning site). The inset displayed Fig. 4 details each of these events. The process is repeated until the domain wall is pinned to the desired defect site (here, the final pinning site at $x = 100$, representing level 7 with binary code 111). Under the condition of zero strain and for the transition wave pinned at an arbitrary defect site, the position of the domain wall – thus, the memory state – may be determined from the time of flight of a small-amplitude
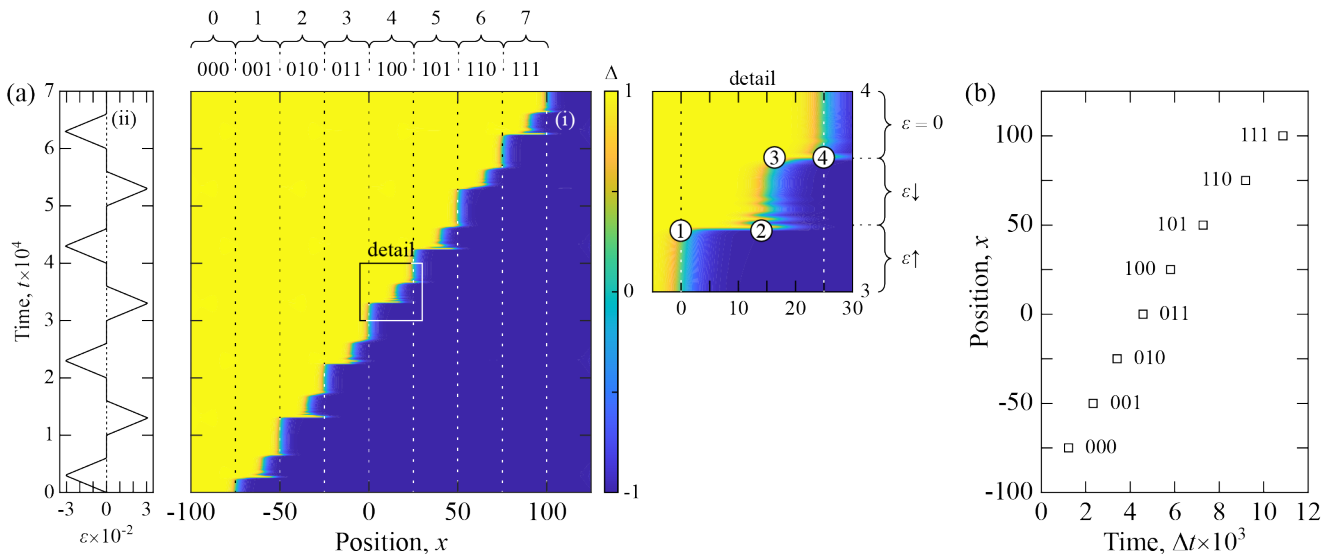
FIG. 4. Mechanical multi-level Memory Performance. (a) (i) The spatio-temporal evolution of the configuration, Δ, in the memory element subject to (ii) a periodic schedule of of compressive, tensile, and zero strain. Detail of (i) shows the domain wall ① de-pinning and mobilization from a (permanent) soft defect at $x = 0$, and ② re-pinning, respectively, within (temporary) local energy minima developed under increasing strain (i.e., $\varepsilon \uparrow$). As the strain decreases (i.e. $\varepsilon \downarrow$), ③ the gradient in ψ enforced by α drives the transition wave ④ to the soft defect pinning site at $x = 25$. (b) Correlation between the domain wall pinned position (syn., binary memory state) and the elapsed time, Δt, between the injection and echo of a harmonic pulse.

signal injected into the metamaterial with appropriate carrier frequency. Figure 4b shows the results of such an exercise conducted in the numerical model when the transition wave is pinned at each of the eight defect sites where the more extended times correspond to higher memory state.

Since $\gamma < 0$ and j_0 places a strain-induced local energy maximum and minimum, respectively, before and after each pinning site, the transition wave is restricted to unidirectional motion from left to right. Consequently, to return the system to the inactive phase, Δ_{s1}, a kink may be established at $x = -75$ and conveyed across the memory element by a similar cyclic prescription of strain (Fig. 5). The complete process is animated in Mov. S1.

In summary, we have devised a mechanical system within which the position of a transition wavefront can be precisely controlled and remotely determined, which we exploit for mechanical multi-level memory; yet, energy harvesting and post-fabrication tuning of mechanical properties represent additional opportunities. A realization of the proposed memory architecture may find application in soft robotics, providing a flexible (albeit, rudimentary) alternative to current, ceramic-based technologies. As the essential characteristics – multi-stability, soft defects, and the proportional relationship among stiffnesses – are independent of scale, the proposed design, leveraging advancements in 3D-printing, is amenable to later efforts aimed at increasing memory density via miniaturization.

See supplementary material for further details of equation derivations and an animation of the

strain-induced transition wave motion exhibited in Fig. 4.

The data that supports the findings of this study are available within the article and its supplementary

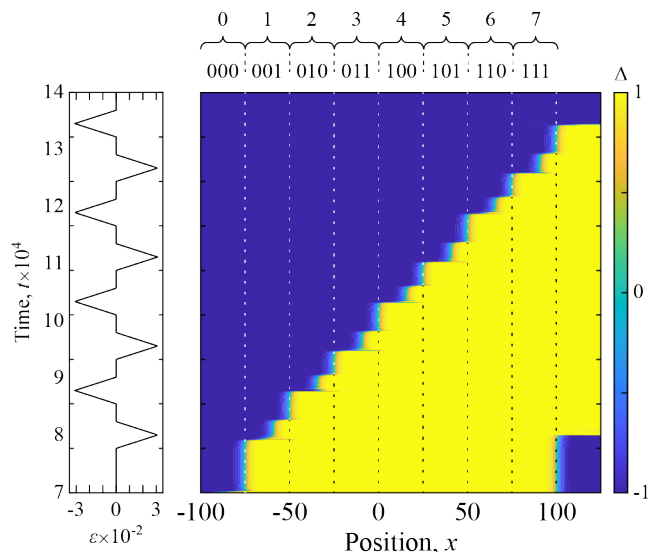
FIG. 5. Memory Reset. The memory is reset by initializing and advancing a kink. Here, we prescribe an initial velocity, $\dot{v}_1 = -0.6148$, to create the kink, and then, following a settling period, advance the kink via the cyclic application of strain.

material.

[1] V. K. Wadhawan, *Introduction to Ferroic Materials*. CRC Press, 1st ed., 2000. ISBN: 9789056992866.

[2] T. H. E. Lahtinen, K. J. A. Franke, and S. van Dijken, "Electric-field control of magnetic domain wall motion and local magnetization reversal," *Sci. Rep.*, vol. 2, p. 258, February 2012.

[3] G. Catalan, J. Seidel, R. Ramesh, and J. F. Scott, "Domain wall nanoelectronics," *Rev. Mod. Phys.*, vol. 84, pp. 119–156, February 2012.

[4] M. Hayashi, L. Thomas, R. Moriya, C. Rettner, and S. S. P. Parkin, "Current-controlled magnetic domain-wall nanowire shift register," *Science*, vol. 320, pp. 209–211, April 2008.

[5] J. A. Mundy, J. Schaab, Y. Kumagai, A. Cano, M. Stengel, I. P. Krug, D. M. Gottlob, H. Doganay, M. E. Holtz, and R. Held, "Functional electronic inversion layers at ferroelectric domain walls," *Nat. Mater.*, vol. 16, pp. 622–627, June 2017.

[6] J. Schaab, S. H. Skjaervo, S. Krohns, X. Dai, M. E. Holtz, A. Cano, M. Lilienblum, Z. Yan, E. Bourret, and D. A. Muller, "Electrical half-wave rectification at ferroelectric domain walls," *Nat. Nanotechnol.*, vol. 13, pp. 1028–1034, November 2018.

[7] D. M. Kochmann and K. Bertoldi, "Exploiting microstructural instabilities in solids and structures: from metamaterials to structural transitions," *Appl. Mech. Rev.*, vol. 69, p. 050801, September 2017.

[8] N. Nadkarni, C. Daraio, R. Abeyaratne, and D. M. Kochmann, "Universal energy transport law for dissipative and diffusive phase transitions," *Phys. Rev. B*, vol. 93, p. 104109, March 2016.

[9] N. Nadkarni, A. F. Arrieta, C. Chong, D. M. Kochmann, and C. Daraio, "Unidirectional transition waves in bistable lattices," *Phys. Rev. Lett.*, vol. 116, p. 244501, June 2016.

[10] M. Hwang and A. F. Arrieta, "Solitary waves in bistable lattices with stiffness grading: augmenting propagation control," *Phys. Rev. E*, vol. 98, p. 042205, October 2018.

[11] B. Deng, P. Wang, V. Tournat, and K. Bertoldi, "Nonlinear transition waves in free-standing bistable chains," *J. Mech. Phys. Solids*, vol. 136, p. 103661, March 2020.

[12] V. Ramakrishnan and M. J. Frazier, "Transition waves in multi-stable metamaterials with space-time modulated potentials," *Appl. Phys. Lett.*, vol. 117, p. 151901, October 2020.

[13] H. Yasuda, L. M. Korpas, and J. R. Raney, "Transition waves and formation of domain walls in multistable mechanical metamaterials," *Phys. Rev. Applied*, vol. 13, p. 054067, May 2020.

[14] L. Jin, R. Khajehtourian, J. Mueller, A. Rafsanjani, V. Tournat, K. Bertoldi, and D. M. Kochmann, "Guided transition waves in multistable mechanical metamaterials," *Proc. Natl. Acad. Sci.*, vol. 17, pp. 2319–2325, January 2020.

[15] A. Zareei, B. Deng, and K. Bertoldi, "Harnessing transition waves to realize deployable structures," *Proc. Natl. Acad. Sci.*, vol. 117, pp. 4015–4020, February 2020.

[16] B. Deng, M. Zanaty, A. E. Forte, and K. Bertoldi, "Topological solitons make metamaterials crawl," *Phys. Rev. Appl.*, vol. 17, p. 014004, January 2022.

[17] D. Melancon, A. E. Forte, L. M. Kamp, B. Gorissen, and K. Bertoldi, "Inflatable origami: multimodal deformation via multistability," *Adv. Funct. Mater.*, p. 2201891, June 2022.

[18] A. P. Browning, F. G. Woodhouse, and M. J. Simpson, "Reversible signal transmission in an active mechanical metamaterial," *Proc. R. Soc. A*, vol. 475, p. 20190146, July 2019.

[19] V. Ramakrishnan and M. J. Frazier, "Multistable metamaterial on elastic foundation enables tunable morphology for elastic wave control," *J. Appl. Phys.*, vol. 127, p. 225104, June 2020.

[20] J. R. Raney, N. Nadkarni, C. Daraio, D. M. Kochmann, J. A. Lewis, and K. Bertoldi, "Stable propagation of mechanical signals in soft media using stored elastic energy," *Proc. Natl. Acad. Sci.*, vol. 113, pp. 9722–9727, 2016.

[21] P. Bhovad and S. Li, "Physical reservoir computing with origami and its application to robotic crawling," *Sci. Rep.*, vol. 11, p. 13002, June 2021.

[22] B. Treml, A. Gillman, P. Buskohl, and R. Vaia, "Origami mechanologic," *Proc. Natl. Acad. Sci.*, vol. 115, pp. 6916–6921, July 2018.

[23] T. Chen, M. Pauly, and P. M. Reis, "A reprogrammable mechanical metamaterial with stable memory," *Nature*, vol. 589, pp. 386–390, January 2021.

[24] N. Nadkarni, C. Daraio, and D. M. Kochmann, "Dynamics of periodic mechanical structures containing bistable elastic elements: From elastic to solitary wave propagation," *Phys. Rev. E*, vol. 90, p. 023204, August 2014.

[25] G. Noh and K.-J. Bathe, "An explicit time integration scheme for the analysis of wave propagations," *Comput. Struct.*, vol. 129, pp. 178–193, August 2013.